Proceedings of the 28th IEEE
EMBS Annual International Conference
New York City, USA, Aug 30-Sept 3, 2006

A reliability study of fractal analysis of the skeletonised vascular network using the "box-counting" technique

T. J. MacGillivray and N. Patton

***Abstract*—Binary vascular networks of the human retina were obtained by computerized processing of digital fundus images. Fractal analysis was performed on skeletonised versions. The effect of three parameters in the vascular segmentation and skeletonization algorithm was quantified, with threshold level found to have the greatest influence. The results were compared to fractal analysis of skeletons derived by manual tracing. The mean difference in fractal dimension between 2 observers is 0.004 (0.3%) and the coefficient of repeatability is ±0.050 (3.4%). Between a single observer and the computerized approach the mean difference is 0.012 (0.8%) and the coefficient is ±0.038 (2.6%). The computerized approach demonstrated a superior reliability compared to manual segmentation.**

I. Introduction

EXAMINATION of the human retinal vasculature may reveal diabetes, hypertension, cardiovascular disease and stroke [1, 2]. Fractal analysis provides a method for the quantitative study of changes to the vascular network [3, 4, 5]. This may be of use in the early detection of vascular change as well as enabling an insight into the progression of disease processes.

Previous fractal work centered on vessel patterns traced by hand, the gold standard for segmenting anatomical structures in retinal images but a time consuming activity. Many computerized algorithms have been proposed for vascular segmentation, making use of adaptive filtering, morphology, and tracking techniques [6, 7, 8, 9]. We have implemented a procedure described in Heneghan *et al.* [10]. The technique was fairly straightforward to apply and uses morphological filters to highlight linear structures while the differential properties of vessels provide additional emphasis. We then skeletonise the segmented network to generate a geometric object for fractal analysis

Fractal analysis was applied to vascular networks determined by both manual and computerized segmentation methods, and we studied the reliability of fractal dimension measurements to gauge its potential usefulness as a sensitive marker for vascular change.

In the rest of this paper we describe the processing and analysis algorithms and present the results of the reliability study.

Manuscript received July 10, 2006.

T. J. MacGillivray is with the Clinical Research Facility, Western General Hospital, University of Edinburgh, Edinburgh EH4 2XU, UK (corresponding author - phone: +44(0)131 537 3351; fax: +44(0)131 535 3361; e-mail: t.j.macgillivray@ed.ac.uk).

N. Patton is with the Princess Alexandra Eye Pavilion, NHS Lothian University Hospitals Division, Edinburgh EH3 9HA, UK.

II. Image Processing

A. Segmentation

Vascular network segmentation was performed on the Green channel of digital colour fundus images as this typically exhibits the greatest contrast. The algorithm was implemented using Matlab (The Mathworks Inc., USA).

The first step is morphological filtering which is used to accentuate the vasculature and preserve vessel crossings and bifurcations. Consider an image $I_0(x, y)$ which is the negative of the Green channel image. Noise and non-vessel structures are removed by taking the supremum of the openings of I_0 with a linear structuring element at several different rotations. Some small detail lost in this process is recovered by morphological reconstruction [11]. The combined operation is

$$I_c = R_{I_0}\left(\sup_{i=1,\ldots 12}\left\{\gamma_{B_i}(I_0)\right\}\right) \qquad (1)$$

where γ_{Bi} denotes the opening of an image with structuring element B at rotation i. 12 rotations each 15° apart are used. R denotes morphological reconstruction, where the supremum of the openings is the marker image and I_0 the mask.

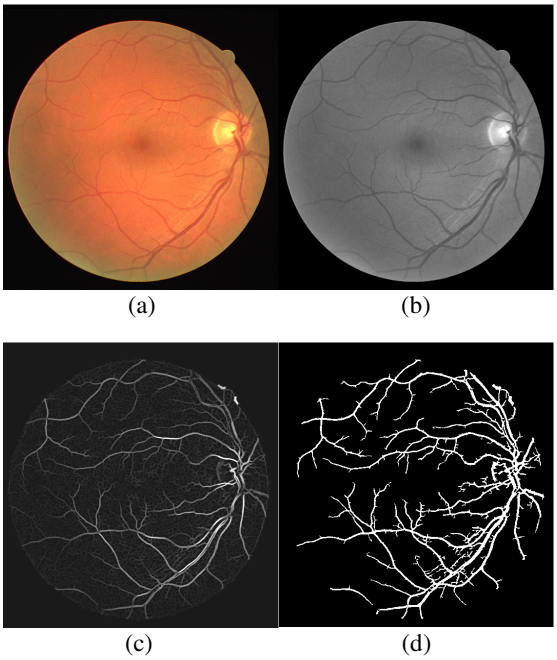

(a) (b) (c) (d)

Fig. 1. (a) Colour fundus image. (b) Green channel image. (c) After morphological filtering and processing. (d) After *Hysteresis Thresholding*.

By taking the infimum of openings of I_0 with a linear structuring element B at 12 rotations each 15°, the background image is obtained,

$$I_b = \inf_{i=1,\ldots 12} \{\gamma_{B_i}(I_0)\}. \quad (2)$$

Subtracting I_b from I_c generates an image I_v containing only linear shapes, i.e. mostly vessels.

The vessel cross-sectional greyscale profile has an approximately Gaussian or double-Gaussian shape [2]. Taking the negative of the second derivative of this will brighten the vessel while other structures are darkened. In a number of cross sectional directions, the true vessel cross-section gives the strongest response. Hence the supremum is taken. Smoothing with a Gaussian filter prevents the vessel boundaries from becoming jagged by the second derivative calculation. The combined operation can be expressed as

$$I_{diff} = \sup_{\theta=0,\ldots 180} \{I_v * G_\theta * (G''_{\theta+90})\} \quad (3)$$

where G_θ denotes the 1D Gaussian convolution kernel at an angle θ^o and $G''_{\theta+90}$ denotes the 1D second derivative of the Gaussian convolution kernel (the Laplacian-of-Gaussian) at an angle $(90+\theta)^o$.

Equation (3) can result in the brightening of edges of flat regions due to rapid changes in brightness. These non-vessel areas are removed by application of the morphological filter in (1) to I_{diff} yielding an image I_l. Also, wide vessels can appear dark in the middle compared to vessel edges as the Gaussian profile approximation is no longer completely valid. These dark areas are removed by

$$I_f = R^*_{I_l}(\inf_{i=1,\ldots 12} \{\phi_{B_i}(I_l)\}) \quad (4)$$

where the filter uses closings instead of openings, takes the infimum instead of the supremum, and reconstruction is reconstruction by erosion (denoted by R^*). The final processed image, I_f, is displayed in Fig. 1 (c).

The vascular network is a tree-like structure. *Hysteresis Thresholding* is used to produce the binary vascular network image as it exploits this property [12]. Two binary images are created; I_{low} by thresholding I_f with a low threshold t_{low}, and I_{high} by thresholding with a higher threshold value t_{high}. I_{high} is then reconstructed into I_{low}, i.e. I_{high} is the marker image and I_{low} the mask. The generated output network image, as shown in Fig 1 (d), marks pixels white if they are part of vessels and black everywhere else.

To skeletonize the vascular network for fractal analysis we adopted Matlab's skeletonization algorithm *bwmorph* which is based on iterative deletion of pixels, preserving the 8-neighbour connectivity information [13]. The skeleton contains many small branches, some of which correspond to noise. To remove noisy elements, we "tidy" the skeleton by first pruning to remove p pixels from each branch, storing branches that are removed in I_{rem}. Then the end points of the pruned skeleton, I_{ends}, are found. Reconstructing I_{ends} into I_{rem} U I_{ends} recovers only branch parts that came from branches not completely removed by pruning. Adding recovered branch ends to the pruned skeleton gives the final filtered skeleton. The outcome of skeletal filtering is the removal of all branches shorter than p pixels while longer branches are left unchanged. Fig. 2 illustrates the results of the skeletonisation process.

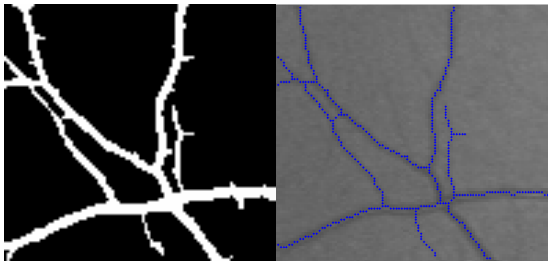

(a) (b)

Fig. 2. (a) A section (100 pixels x 100 pixels) of the segmented binary vascular network. (b) Skeleton of binary network (blue) overlaid on corresponding section of the Green channel image.

B. Fractal Analysis

We employ *box-counting* to determine the fractal dimension of the skeleton [4]. The skeleton image is overlaid with a series of boxes of decreasing size. The step number, n, determines the sizes of the boxes. For example, the corresponding step number series for an image 512 pixels by 512 pixels would be n = 0, 1, 2, …9 and the box sizes are then $s = 512/2^n$. The number of boxes, N, containing at least one white (skeleton) pixel is counted for each box size in the series. The value of the least squares regression slope of the plot of *ln(N) versus n*ln(2)* yields the estimate of fractal dimension, D_f. See Fig. 3 where the value of the slope and hence the estimate of D_f is 1.443 for the image in Fig. 1.

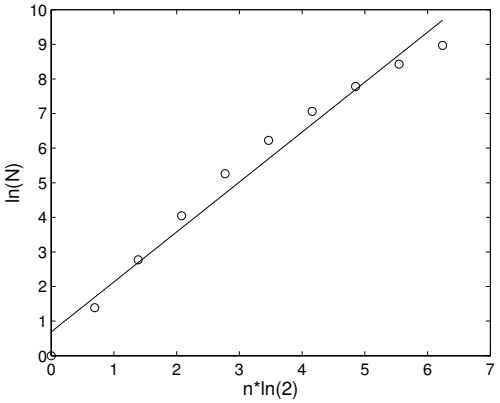

Fig. 3. Plot of *ln(N) versus n*ln(2)* and best fit straight line calculated by least squares method.

III. RESULTS

The segmentation algorithm and fractal analysis procedure were tested on the publicly available DRIVE set by Staal et al [9]. The images were acquired using a Canon CR5 non-mydriatic 3CCD camera with a 45° field of view (FOV). Each image was captured using 8 bits per color plane at 768 pixels by 584 pixels. The FOV of each image is circular with a diameter of approximately 540 pixels.

The photographs were from a diabetic retinopathy screening program.

We investigated the effect of adjusting various parameters in the segmentation algorithm on the measured fractal dimension for DRIVE image *01_test.tif*. Adjustable input parameters include the size of the structuring element in morphological filtering, low and high values in *Hysteresis Thresholding*, and the prune number for skeletal filtering.

In order to simplify the study on the effect of thresholding we set $t_{low} = t_{high} = T_h$. The size of the structuring element, B, was set to 15 pixels and the prune number, p, to 10 pixels. T_h was varied from 0.03 to 0.15 and D_f of the resulting vascular network skeleton calculated. Fig 4. shows the plot of T_h *versus* D_f . A threshold value of T_h = 0.065 (i.e. a greyscale of 16.575) was found, by visual observation, to give a very good segmentation for the vascular network in the fundus image. A lower value picks up unwanted choroidal vessels while a higher value excludes some of the main vessels.

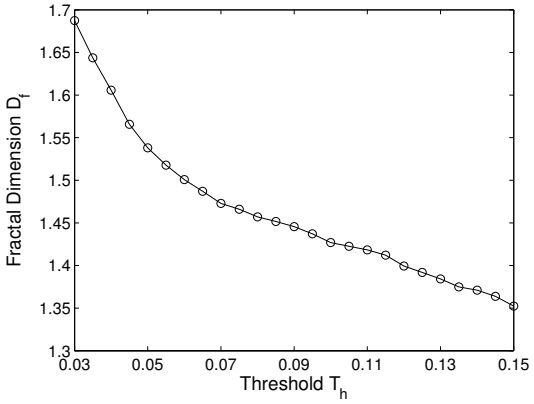

Fig. 4. Variation of fractal dimension, D_f, with threshold, T_h.

The behaviour of the T_h curve is as expected. As T_h increases less of the processed image is included in the binary network image (i.e. vessels are missed off) and the resulting skeleton has an increasingly lower fractal dimension. Over the range of T_h considered, D_f changes by 25 %. A change in T_h of only 0.005 (i.e. a greyscale of 1.275) can result in a change in D_f of up to 3 %.

Using a fixed threshold of T_h = 0.065, the effect of other parameters on D_f was assessed. If the length of B is chosen anywhere in the region of 12 to 16 pixels, the measurement of D_f remains relatively constant, D_f = 1.483±0.008. If the structuring element size is increased, only long straight sections of vessels are segmented. If the size is decreased only very narrow vessels are detected.

Prune number, p, was varied from 0 to 20. The resulting plot of p *versus* D_f is shown in Fig 5. Over the range of values considered, D_f drops by 3 %. With a change in p of ±1, D_f changes by a maximum of 0.3 %. Prune number has a very small affect of the skeleton and hence D_f. Increasing p removes more points or branches from the skeleton thus decreasing D_f.

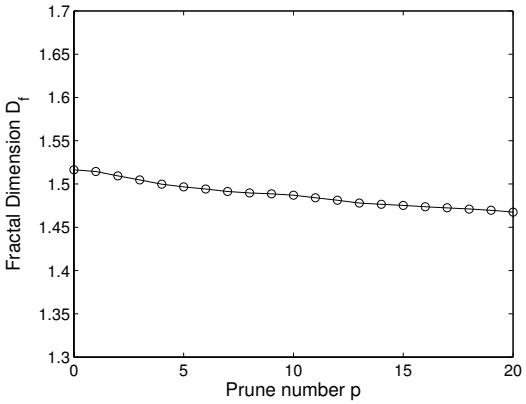

Fig. 5. Variation of fractal dimension, D_f, with prune number, p.

Two sets of manual segmentations for the fundus images are also available in the DRIVE database. These sets were created after 2 human observers were asked to mark all pixels in the fundus images for which they were at least 70 % certain belonged to vessels. We produced skeletons for the manually segmented images and measured the fractal dimension using the *box-counting* technique. We then produced our own segmented images using the algorithm, computed the skeleton and measured fractal dimension. The results are given in Table 1.

TABLE I
MEASUREMENTS OF FRACTAL DIMENSION

Image	1st manual segmentation	2nd manual segmentation	algorithm segmentation
1	1.480	1.483	1.499
2	1.482	1.473	1.455
3	1.478	1.453	1.468
4	1.472	1.466	1.434
5	1.485	1.453	1.457
6	1.498	1.504	1.481
7	1.471	1.433	1.460
8	1.465	1.436	1.481
9	1.467	1.483	1.433
10	1.474	1.439	1.476
11	1.502	1.483	1.467
12	1.467	1.464	1.456
13	1.499	1.484	1.451
14	1.459	1.450	1.446
15	1.441	1.434	1.454
16	1.468	1.481	1.440
17	1.451	1.448	1.449
18	1.438	1.465	1.443
19	1.461	1.492	1.465
20	1.431	1.492	1.423

Bland Altman plots (see Fig. 6 and Fig. 7) were used to compare fractal dimension measurements derived from the different segmentations [14]. Both plots show a random scatter of points. The mean difference between D_f derived from manually segmented images for 2 observers is 0.004 and the coefficient of repeatability is ±0.050. The mean difference between D_f derived from the first set of manually segmented images and from the computerized segmentations is 0.012 and the coefficient of repeatability is ±0.038.

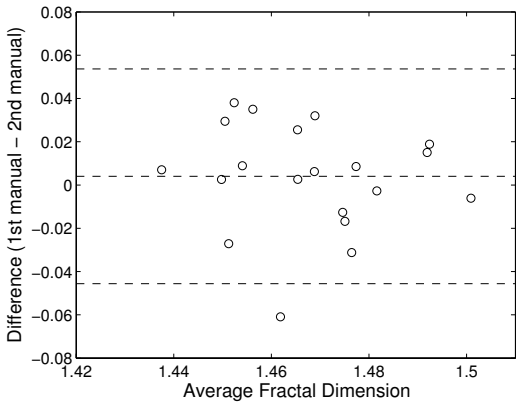

Fig. 6. Bland Altman plot comparing fractal dimension measurements derived from manual segmentations by 2 observers.

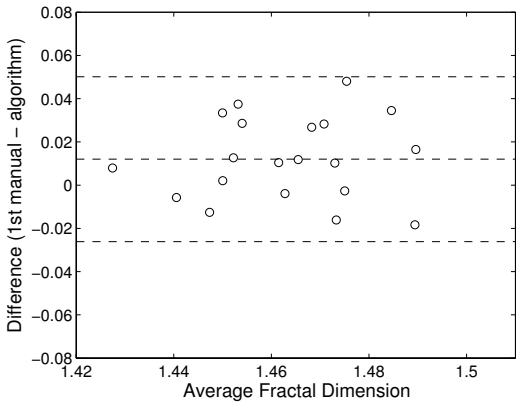

Fig. 7. Bland Altman plot comparing fractal dimension measurements derived from manual and computerized segmentations.

IV. DISCUSSION

Threshold level was found to have the largest influence on fractal dimension as it greatly affects the computerized segmentation. The other parameters also affect segmentation and hence fractal dimension but not as significantly as threshold level. Variations in fractal dimension measurements derived from the two manual segmentations will be due to differences in the individual tracings made by each observer. Some of the differences in fractal dimension derived from manual and computerized methods are related to problems with the segmentation algorithm. The edge of the optic disk is often incorrectly segmented as a vessel. Some vessels with low contrast relative to the background are missed. Spurious side spurs are detected off major vessels. Underlying choroidal vessels are sometimes incorrectly segmented. Darks areas in the middle of vessels are sometimes not properly filled in. Sections of the FOV boundary are sometimes mistakenly segmented.

A more rigorous assessment of the segmentation algorithm and its performance is now required. This will allow artefacts to be identified and removed thus helping to improve computerized segmentation and its use in fractal analysis.

V. CONCLUSION

Fractal analysis of the human vascular network segmented by computerized process is achievable. We found that the coefficient of repeatability was less for the observer versus computer than for the two observers. Therefore, there was greater precision with the computerized method when compared to the inter-observer study. We have demonstrated non-inferiority of computerized segmentation for measuring fractal dimension. The computerized segmentation exhibited superior reliability compared to manual segmentation. Further investigation is now worthwhile to establish the sensitivity of fractal analysis as a marker of vascular change.

REFERENCES

[1] T. Y. Wong, R. K. Klein, B. E. K. Klein, J. M. Tielsch, L. Hubbard, F. J. Nieto, "Retinal microvascular abnormalities and their relationship with hypertension, cardiovascular disease, and mortality", *Survey of Ophthalmology*, vol. 46, no. 1, 2001.

[2] N. Patton, T.M. Aslam, T.J. MacGillivray, I.J. Deary, B. Dhillon, R.H. Eikelboom, K. Yogesan, I.J. Constable, "Retinal image analysis: concepts, applications and potential", *Prog. Retin. Eye Res.*, vol. 25, no. 1, pp. 99-127, 2006.

[3] A. Daxer, "Characterisation of the neovascularisation process in diabetic retinopathy by means of fractal geometry: diagnostic implications", *Clinical and Experimental Ophthalmology*, vol. 231, pp. 681-686, 1993.

[4] A. Avakian, R. E. Kalina, E. H. Sage, A. H. Rambhia, K. E. Elliott, E. L. Chuang, J. I. Clark, J. Hwang and P. Pasons-Wingerter, "Fractal analysis of region-based vascular changes in the normal and non-proliferative diabetic retina", *Current Eye Research*, vol. 24, no. 4, pp. 274-280, 2002.

[5] B. R. Masters, "Fractal analysis of the vascular tree in the human retina", *Annu. Rev. Biomed Eng*, vol. 6, pp. 427-52, April 2004.

[6] F. Zana and J. Klein, "Robust segmentation of vessels from retinal angiography", in *Proc. Int. Conf. Digital Signal Processing*, pp. 1087-1091, 1997.

[7] L. Gang, O. Chutatape and S. M. Krishnan, "Detection and measurement of retinal vessels in fundus images using amplitude modified second-order Gaussian filter", *IEEE Trans. Biomedical Engineering*, vol. 69, pp. 168-172, 2002.

[8] L. Gagnon, M. Lalonde, M. Beaulieu, M. Boucher, "Procedure to detect anatomical structures in optical fundus images", in *Proc. Conf. Medical Imaging 2001: Image Processing*, pp. 1218-1225.

[9] J. J. Staal, M. D. Abramoff, M. Niemeijer, M. A. Viergever, B. van Ginneken, "Ridge based vessel segmentation in color images of the retina", *IEEE Transactions on Medical Imaging*, vol. 23, pp. 501-509, 2004.

[10] C. Heneghan, J. Flynn, M. O'Keefe and M. Cahill, "Characterization of changes in blood vessel width and tortuosity in retinopathy of prematurity using image analysis", *Medical Image Analysis*, vol. 6, no. 4, pp. 407-429, December 2002.

[11] R. C. Gonzalez, R. E. Woods and S. L. Eddins, *Digital Image Processing Using Matlab*, Pearson Prentice Hall, 2004.

[12] J. Canny, "A computational approach to edge detection", *IEEE Tran.s Pattern Analysis Machine Intelligence*, vol. 8, no. 1, pp. 62-67, 1979.

[13] L. Lam., S.-W. Lee, and C. Y. Suen, "Thinning methodologies - a comprehensive survey," *IEEE TPAMI*, vol. 14, no. 9, pp. 869-885, 1992.

[14] J. M. Bland and D. G. Altman, "Statistical methods for assessing agreement between two methods of clinical measurement", *The Lancet*, pp. 307-310, February 1986.